

Efficient Epipolar Consistency

André Aichert, Katharina Breininger, Thomas Köhler and Andreas Maier

Pattern Recognition Lab, Friedrich-Alexander Universität Erlangen-Nürnberg, Germany

Abstract—Epipolar consistency has been shown to be a powerful tool in calibration and motion correction for both flat panel detector CT (FD-CT) and other X-ray based applications. The epipolar consistency Conditions apply to projection data directly and can be used to correct for 3D parameters without 3D reconstruction. The computation of an epipolar consistency metric is real-time capable for small sets of images and can be parallelized for large sets of images. It has been shown to correct for motion in FD-CT scans in under one minute. This work presents a straight-forward and efficient implementation of the epipolar consistency metric. It shows that most of the algorithm is linear and can, in fact, be reduced to two 3×2 matrix-vector products by analytic simplification. This paper presents a full algorithm along with a brief validation of a GPU implementation. Said implementation is available as MATLAB source code to facilitate the application of Epipolar consistency to a variety of problems by other groups.

I. INTRODUCTION

Consistency conditions in CT have been studied for decades. Yet, their practical application remains limited by hard assumptions on the imaging geometry (e.g. fan-beam only) and trajectory (e.g. full circle). Debbeler et al. [1] presented a raw data redundancy metric in 2013, which was later reformulated by Aichert et al. [2] to the epipolar consistency Conditions (ECC). Earlier work exists, which derives a similar set of consistency conditions from John’s equation [3]. Not only is this consistency metric efficient to compute, it was also shown to be applicable to any set of X-ray projections, no matter the type and shape of trajectory (circular, saddle, circle and line to name a few), as long as the images showed the same part of the same object. Recent work by Maass et al. [4] and Fryscht et al. [5] shows that ECC have practical applications for calibration and motion correction in flat detector CT and is fast enough to support clinical applications. It has also been suggested to apply ECC to other X-ray based modalities including fluoroscopy [6] and tomosynthesis [7].

This paper reviews the ECC algorithm presented in [6] to compute the epipolar consistency metric and further simplifies it, presenting an efficient and easily repeatable implementation. The paper presents both pseudo-code and a MATLAB implementation to estimate the relative geometry between two X-ray projections. Its extension to FD-CT is then merely an application of the presented algorithm to all pairs of projections of the scan. We hope that this paper allows other groups to apply the ECC to their problems and possibly find new applications.

II. REVIEW OF EPIPOLAR CONSISTENCY ALGORITHM

A. Overview

This section provides mathematical tools and summarizes an algorithm to compute a metric of epipolar consistency. We consider two transmission-only projections I_0 and I_1 , where each image point contains an integral over absorption coefficients along a ray through space. We denote the respective projection matrices as \mathbf{P}_0 and $\mathbf{P}_1 \in \mathbb{R}^{3 \times 4}$ with corresponding finite source positions $\mathbf{C}_0 \cong (C_0^0, C_0^1, C_0^2, 1)^\top \propto \text{null}(\mathbf{P}) \in \mathbb{P}^3$ and \mathbf{C}_1 accordingly, in homogeneous coordinates of oriented projective three-space, where \cong denotes an equivalence relation up to positive scalar multiples.

The gist of epipolar consistency is that the baseline \mathbf{B} connecting the two source positions \mathbf{C}_0 and \mathbf{C}_1 defines a pencil of planes. By intersection with the detectors, each plane defines two lines \mathbf{l}_0 and $\mathbf{l}_1 \in \mathbb{P}^2$ in the projection images I_0 and I_1 . These lines are well known from Computer Vision as epipolar lines. In case of transmission-based modalities such as X-ray imaging, both lines go back to the absorption of the same plane through the object and therefore “contain” the same total absorption. In parallel geometries, i.e. if the source positions \mathbf{C}_0 and \mathbf{C}_1 are at infinity, an integral over the line \mathbf{l}_0 should be identical to an integral over the line \mathbf{l}_1 , provided there is no truncation of the object. We can use Grangeat’s theorem to generalize for arbitrary projections, which introduces a derivative in orthogonal direction to the lines [8]. Note that our work consistently and successfully ignores certain cosine weights, which are, however, addressed in [1], [4].

The ECC algorithm consists of the following major steps. 1) Pre-processing: First, the derivative orthogonal

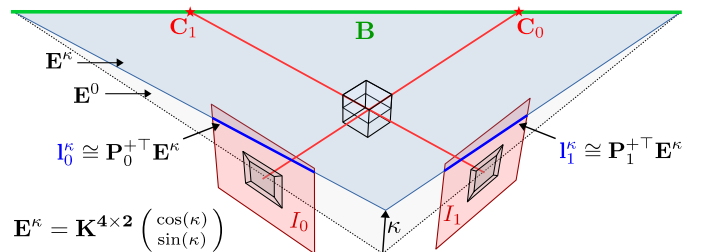


Figure 1. Epipolar geometry of two cone-beam projection images with projection matrices $\mathbf{P}_0, \mathbf{P}_1 \in \mathbb{R}^{3 \times 4}$. The source positions $\mathbf{C}_0, \mathbf{C}_1 \in \mathbb{P}^3$, along with the principal rays orthogonal to the detectors I_0 and I_1 are shown in red. The epipolar plane \mathbf{E}^κ (light blue) intersects the reference plane \mathbf{E}^0 (light gray) in the baseline (green) at an angle κ . The corresponding epipolar lines $\mathbf{l}_0^\kappa, \mathbf{l}_1^\kappa \in \mathbb{P}^2$ are the points of intersection on the detectors with the plane \mathbf{E}^κ .

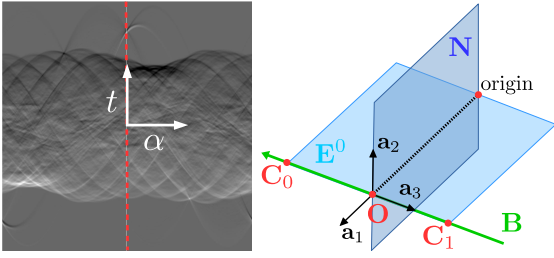


Figure 2. Left: Derivative $\frac{\partial}{\partial t}\rho_I(\alpha, t)$ of the Radon transform of an image I . Note the symmetry w.r.t. a change in angle by 180° $\frac{\partial}{\partial t}\rho_I(\alpha, t) = -\frac{\partial}{\partial t}\rho_I(\alpha + \pi, -t)$. Right: The three vectors \mathbf{a}_1 , \mathbf{a}_2 and \mathbf{a}_3 form an orthogonal basis, where the vectors \mathbf{a}_1 and \mathbf{a}_2 span the plane \mathbf{N} , which contains the origin and is orthogonal to baseline \mathbf{B} connecting the source positions \mathbf{C}_0 and \mathbf{C}_1 .

to the lines of the Radon transform of all projection images is computed, compare Section II-B. 2) Geometry: Second, the geometric part of the algorithm finds a mapping from an angle κ that parametrizes the bundle of planes around the baseline to two lines, with redundant information, compare Section II-C. 3) Sampling: Third, the two epipolar lines are converted to angle α to the x -axis and signed distance to the origin t . The pre-computed Radon derivatives are then sampled at corresponding locations (α, t) , compare Section II-D. The last steps are repeated for all angles κ with some spacing $d\kappa$ and the sum of squared differences of the redundant values is computed and returned. This paper addresses only the computation of a consistency metric. Calibration and motion correction can be done numerically optimizing said metric over parameters of the projection geometry.

B. Algorithm: Derivative of the Radon Transform

The ECC compare the integrals of corresponding lines in projection images. Debbeler et al. [1] suggests pre-computing the integrals of all lines $\mathbf{l} \cong (-\sin(\alpha), \cos(\alpha), -t)^\top$ using the Radon transform $\rho_I(\alpha, t)$ of a projection image I . This is the most important optimization in the ECC algorithm, because we need to compare thousands of line-integrals. Once the Radon transform is computed, we can sample it, instead of repeatedly computing similar line integrals. The Radon transform is well-known in the CT community as the parallel-beam forward projector in two dimensions. In this case, however, it is computed from a cone-beam projection image. Care should be taken for the Radon transform to have sufficient bins, so as to avoid under-sampling. As a rule of thumb, the Radon transform should have at least as many bins as the input image has pixels. The 1st derivative $\frac{\partial}{\partial t}\rho_I(\alpha, t)$ in orthogonal direction to the lines t , can be done, for example, using a Sobel filter, see Figure 2, left. The rest of the ECC algorithm is to iterate over an angle κ that parametrizes the pencil of epipolar planes and sample the Radon derivatives in the appropriate places to measure their difference.

C. Algorithm: Parametrizing Epipolar Lines

The epipolar geometry of two images is closely related to the mathematics of the fundamental matrix. Our algorithm, however, uses the underlying concept of Plücker matrices directly [9]. This section summarizes how to find a matrix

$$\mathbf{K} \cong [\tilde{\mathbf{B}}]_{\times} \mathbf{A} = [\tilde{\mathbf{B}}]_{\times} \begin{pmatrix} \mathbf{a}'_1 & \mathbf{a}'_2 & \mathbf{O} \\ 0 & 0 & 0 \end{pmatrix}, \quad (1)$$

which maps a vector $\mathbf{x}^\kappa = (\cos(\kappa), \sin(\kappa), 1)^\top$ to an epipolar plane $\mathbf{E}^\kappa = \mathbf{K} \cdot \mathbf{x}^\kappa \in \mathbb{P}^3$ which intersects the reference plane $\mathbf{E}^0 \in \mathbb{P}^3$ in the baseline at an angle κ , according to Algorithm 1 in [8].

The Plücker coordinates of the baseline \mathbf{B} through the source positions \mathbf{C}_0 and \mathbf{C}_1 are

$$\mathbf{B} \cong (B_{01}, B_{02}, B_{03}, B_{12}, B_{13}, B_{23})^\top, \quad (2)$$

with $B_{01}B_{23} - B_{02}B_{13} + B_{03}B_{12} = 0$, where

$$\mathbf{B}_{ij} = C_0^i C_1^j - C_1^i C_0^j. \quad (3)$$

The Plücker Matrix $[\mathbf{B}]_{\times}$ and its dual $[\tilde{\mathbf{B}}]_{\times}$ are related via $[\tilde{\mathbf{B}}]_{\times}[\mathbf{B}]_{\times} = \mathbf{0}$. The direction \mathbf{a}_3 of the baseline \mathbf{B} can be computed by multiplication with the plane at infinity $\pi^\infty = (0, 0, 0, 1)^\top$

$$[\mathbf{B}]_{\times} \pi^\infty = \begin{pmatrix} -B_{03} \\ -B_{13} \\ -B_{23} \\ 0 \end{pmatrix} = \begin{pmatrix} \mathbf{a}_3 \\ 0 \end{pmatrix}. \quad (4)$$

The vector \mathbf{a}_3 points in the direction from the point \mathbf{C}_0 to the point \mathbf{C}_1 . The infinite point $\mathbf{N} \cong [\tilde{\mathbf{B}}]_{\times} \pi^\infty = (\mathbf{a}_3, 0)^\top$ can also be interpreted as a plane through the origin. The common plane

$$\mathbf{E}^0 \cong [\tilde{\mathbf{B}}]_{\times} \mathbf{X}^0 \quad (5)$$

of the baseline \mathbf{B} and some reference point \mathbf{X}^0 in the object defines where the plane with $\kappa = 0$ shall lie. Let \mathbf{a}_2 denote the first three components of \mathbf{E}^0 , i.e. its orthogonal. Let \mathbf{O} denote the intersection of the plane \mathbf{N} with the baseline \mathbf{B} . Then, \mathbf{O} is the orthogonal projection of the origin to the baseline and thus its closest point to the origin

$$\mathbf{O} \cong [\mathbf{B}]_{\times} \mathbf{N} \cong [\mathbf{B}]_{\times} [\tilde{\mathbf{B}}]_{\times} \pi^\infty. \quad (6)$$

We finally have $\mathbf{a}'_2 = \frac{\mathbf{a}_2}{\|\mathbf{a}_2\|}$, $\mathbf{a}'_3 = \frac{\mathbf{a}_3}{\|\mathbf{a}_3\|}$ and $\mathbf{a}'_1 = \mathbf{a}'_3 \times \mathbf{a}'_2$.¹ See Figure 2, right, for the geometry of the baseline and the vectors \mathbf{a}_1 , \mathbf{a}_2 , \mathbf{a}_3 .

D. Algorithm: Sampling the Radon Transforms

Given an epipolar plane $\mathbf{E} \in \mathbb{P}^3$ we can find the two epipolar lines

$$\mathbf{l}_0 = \mathbf{P}_0^{+\top} \mathbf{E} \text{ and } \mathbf{l}_1 = \mathbf{P}_1^{+\top} \mathbf{E}, \quad (7)$$

where $\circ^{+\top}$ denotes the pseudo-inverse transpose of a projection matrix. The Radon transform is commonly parametrized by the signed distance to the image center, while the projection images typically have the coordinate origin in one of the corners. We account for this with

¹Sign of \mathbf{a}'_1 determines direction of rotation, which is arbitrary.

Algorithm 1 Epipolar geometry in 12 lines of CUDA, see Section II-C and II-D. `sgemm` is the BLAS matrix multiply.

```

// Plücker coordinates of baseline (vectors a2 and a3):
float B01 = c0[0]*c1[1] - c0[1]*c1[0]; // a2[2]
float B02 = c0[0]*c1[2] - c0[2]*c1[0]; // -a2[1]
float B03 = c0[0]*c1[3] - c0[3]*c1[0]; // a3[0]
float B12 = c0[1]*c1[2] - c0[2]*c1[1]; // a2[0]
float B13 = c0[1]*c1[3] - c0[3]*c1[1]; // a3[1]
float B23 = c0[2]*c1[3] - c0[3]*c1[2]; // a3[2]
// s3 = norm(a3)
float s3 = sqrt( B03*B03 + B13*B13 + B23*B23 );
// K is a 4x2 matrix (column major)
float K[] = {
+ B12*s3, - B02*s3, + B01*s3, 0, // a2*norm(a3)
- B01*B13 - B02*B23, // a1[0]
+ B01*B03 - B12*B23, // a1[1]
+ B02*B03 + B12*B13, // a1[2]
- B12*B12 - B02*B02 - B01*B01 // -norm(a2)^2
};
// left-multiplication with pseudo-inverse transpose
sgemm<3,4,2>(P0invT,K,K0);
sgemm<3,4,2>(P1invT,K,K1);

```

a homography \mathbf{H} , which moves the coordinate origin by $(-\frac{1}{2}n_x, -\frac{1}{2}n_y)^\top$ to the image center. Lines transform contra-variant by its inverse transpose

$$\mathbf{H}^{-\top} = \begin{pmatrix} 1 & & & \\ & \frac{1}{2}n_x & & \\ & & \frac{1}{2}n_y & \\ & & & 1 \end{pmatrix}. \quad (8)$$

We can thus define two matrices

$$\mathbf{K}_0 = \mathbf{H}^{-\top} \mathbf{P}_0^{+\top} \mathbf{K} \text{ and } \mathbf{K}_1 = \mathbf{H}^{-\top} \mathbf{P}_1^{+\top} \mathbf{K}, \quad (9)$$

which map $\mathbf{x}^\kappa = (\cos(\kappa), \sin(\kappa), 1)^\top$ directly to the two corresponding epipolar lines relative to the image center

$$\mathbf{l}_0^\kappa = \mathbf{K}_0 \mathbf{x}^\kappa \text{ and } \mathbf{l}_1^\kappa = \mathbf{K}_1 \mathbf{x}^\kappa. \quad (10)$$

Finally, angles and signed distances have to be computed from the lines' coordinates.

III. SIMPLIFICATION FOR GPU IMPLEMENTATION

A. World Origin as Reference Point

Without loss of generality, this paper considers the case, where the reference plane \mathbf{E}^0 shall pass through the origin. We can thus write down \mathbf{a}_2 explicitly

$$\mathbf{E}^0 \cong [\tilde{\mathbf{B}}]_\times \begin{pmatrix} 0 \\ 0 \\ 1 \end{pmatrix} = \begin{pmatrix} B_{12} \\ -B_{02} \\ B_{01} \end{pmatrix} = \begin{pmatrix} \mathbf{a}_2 \\ 0 \end{pmatrix}. \quad (11)$$

B. Last Column of \mathbf{A} is Zero

Equation 6 defines \mathbf{O} as a point on the baseline \mathbf{B} with

$$[\tilde{\mathbf{B}}]_\times \mathbf{O} = \underbrace{[\tilde{\mathbf{B}}]_\times [\mathbf{B}]_\times [\mathbf{B}]_\times \pi^\infty}_{=0} = \mathbf{0}. \quad (12)$$

We can simplify Equation 1, $\forall \mathbf{x} = (x_0, x_1, x_2) \in \mathbb{R}^3$:

$$\begin{aligned} \mathbf{K}\mathbf{x} &= [\tilde{\mathbf{B}}]_\times \mathbf{A}\mathbf{x} \\ &= [\tilde{\mathbf{B}}]_\times \begin{pmatrix} \mathbf{a}_1 & \mathbf{a}_2 \\ 0 & 0 \end{pmatrix} \begin{pmatrix} x_0 \\ x_1 \end{pmatrix} + \underbrace{[\tilde{\mathbf{B}}]_\times \mathbf{O}}_{=0} \cdot x_2. \end{aligned} \quad (13)$$

Hence the last column \mathbf{O} of the matrix \mathbf{A} can be dropped completely and we only need to find \mathbf{a}_1 and \mathbf{a}_2 . In consequence, we can also drop the last columns of \mathbf{K}_0 and \mathbf{K}_1

and encode the whole geometry in two 3×2 matrices. By multiplication with $(\cos(\kappa), \sin(\kappa))^\top$ for some angle κ we directly obtain two corresponding epipolar lines.

C. Re-writing the Dual Plücker Matrix

Using a 3×3 Plücker matrix $[\mathbf{a}_3]_\times \mathbf{x} = \mathbf{a}_3 \times \mathbf{x}$ we have

$$[\tilde{\mathbf{B}}]_\times = \begin{pmatrix} [\mathbf{a}_3]_\times & \mathbf{a}_2 \\ -\mathbf{a}_2^\top & 0 \end{pmatrix}, \text{ with } [\mathbf{a}_3]_\times = \begin{pmatrix} 0 & -B_{23} & B_{13} \\ B_{23} & 0 & -B_{03} \\ -B_{13} & B_{03} & 0 \end{pmatrix}. \quad (14)$$

Equation 1 becomes

$$\begin{aligned} \mathbf{K}^{2 \times 4} &\cong [\tilde{\mathbf{B}}]_\times \begin{pmatrix} \mathbf{a}_1 & \mathbf{a}_2 \|\mathbf{a}_3\| \\ 0 & 0 \end{pmatrix} \\ &= \begin{pmatrix} [\mathbf{a}_3]_\times & \mathbf{a}_2 \\ -\mathbf{a}_2^\top & 0 \end{pmatrix} \begin{pmatrix} \mathbf{a}_1 & \mathbf{a}_2 \|\mathbf{a}_3\| \\ 0 & 0 \end{pmatrix} \\ &\cong \begin{pmatrix} \mathbf{a}_2 \|\mathbf{a}_3\| & \mathbf{a}_1 \\ 0 & \|\mathbf{a}_2\|^2 \end{pmatrix} \end{aligned} \quad (15)$$

The whole geometry of epipolar consistency is now encoded in the following matrix multiplication

$$\mathbf{E}^\kappa \cong \begin{pmatrix} +B_{12} \|\mathbf{a}_3\| & -B_{13} B_{01} - B_{02} B_{23} \\ -B_{02} \|\mathbf{a}_3\| & +B_{03} B_{01} - B_{12} B_{23} \\ +B_{01} \|\mathbf{a}_3\| & +B_{03} B_{02} + B_{12} B_{13} \\ 0 & -B_{12}^2 - B_{02}^2 - B_{01}^2 \end{pmatrix} \begin{pmatrix} \cos(\kappa) \\ \sin(\kappa) \end{pmatrix}, \quad (16)$$

with $\|\mathbf{a}_3\| = \sqrt{B_{03}^2 + B_{13}^2 + B_{23}^2}$. This is the main result of this paper and can be converted directly into source code. We obtain Algorithm 1.

D. Singularities

Note that the distance of the baseline to the origin can be written as $\frac{\|\mathbf{a}_3\|}{\|\mathbf{a}_2\|}$. This means that the presented optimization has singularities when the baseline \mathbf{B} contains the origin. Nevertheless, this case is easily avoided by a global translation which brings any preferred reference point to the origin. The algorithm above also requires at least one of the source positions to be finite. However, the geometry of the parallel case is simpler and allows for the direct comparison of line integrals[10].

E. Interpretation

The result of Section III is surprisingly compact. We can even interpret the columns of the matrix $\mathbf{K}^{4 \times 2}$ as planes. The plane $\mathbf{E}^0 \cong [\tilde{\mathbf{B}}]_\times \pi^\infty$ is the reference plane, while the epipolar plane

$$\mathbf{E}^{\frac{\pi}{2}} \cong \left(\frac{\mathbf{a}_1}{\|\mathbf{a}_1\|}, \frac{\|\mathbf{a}_3\|}{\|\mathbf{a}_2\|} \right)^\top \cong [\mathbf{B}]_\times [\mathbf{B}]_\times \pi^\infty, \quad (17)$$

is parallel to the \mathbf{a}_2 - \mathbf{a}_3 plane. It is exactly the plane for $\kappa = 90^\circ$. Using the same argument, we can see that the columns of the matrices $\mathbf{K}_0^{3 \times 2} = \mathbf{P}_0^{+\top} \mathbf{K}^{4 \times 2}$ and $\mathbf{K}_1^{3 \times 2} = \mathbf{P}_1^{+\top} \mathbf{K}^{4 \times 2}$ contain the epipolar lines \mathbf{l}_0^0 , $\mathbf{l}_0^{\frac{\pi}{2}}$ and \mathbf{l}_1^0 , $\mathbf{l}_1^{\frac{1}{2}}$, respectively.

Although the epipolar lines depend linearly on the angle κ , their angle in the image is not linear in κ , because the upper 2×2 parts of $\mathbf{K}_0^{3 \times 2}$ and $\mathbf{K}_1^{3 \times 2}$ are generally not orthogonal, or of equal norm.

Algorithm 2 Sampling redundant value $\frac{\partial}{\partial t}\rho_{I_0}$ at I_0^κ , see Section II-D. The function `tex2D` samples a texture `dtr0` in normalized coordinates using linear interpolation.

```

// Find epipolar line on I0 at angle kappa
float x_k = {cos(kappa), sin(kappa)};
sgemm<3,2,1>(K0,x_k,l0);
// Length of normal
float length0=sqrt(l0[0]*l0[0]+l0[1]*l0[1]);
// Angle between line and x-axis (from 0 to 2)
float dtr0_x=atan2(l0[1],l0[0])/Pi+1.0f;
// Signed distance to center (scaled to Radon bins)
float dtr0_y=(l0[2]/length0)/radon_range_t+0.5f;
// Sample Radon derivative textures (dtr)
if (dtr0_x<1.0f)
  sample0+=tex2D<float>(dtr0, 1.f-dtr0_x, 1.f-dtr0_y);
else // account for symmetry: rho(a,t)=-rho(a+Pi,-t)
  sample0-=tex2D<float>(dtr0, 2.f-dtr0_x, dtr0_y);

```

IV. EXPERIMENTS AND RESULTS

We provide an open-source reference implementation of the epipolar consistency metric, in Octave (MATLAB) ². In addition, we evaluated and timed our GPU implementation on a mobile computer with NVIDIA GTX 860M, on an FD-CT short scan with $n = 133$ projections.

1) Pre-processing: We do not discuss the 2D Radon transform. CPU Computation of pseudo-inverse and null-space of $n = 133$ projection matrices and takes < 1 ms.

2) Geometry: In a CT scan with n projections, there are $N = n \cdot \frac{n-1}{2}$ pairs (e.g. $N = 8,778$ for $n = 133$ and $N = 122,760$ for $n = 496$). We must compute \mathbf{K}_0 and \mathbf{K}_1 for each such pair, see Algorithm 1 and Equation 9. Our CUDA kernel uses 28 registers and takes 1.3ms for $n = 496$, which is not much faster than the CPU.

3) Sampling: Most time is spent iterating over all pairs of projection images and over all angles κ to sample redundant values in the Radon derivatives from texture memory. This step benefits the most from palatalization. There are several ways of distributing the problem. The straightforward implementation computes the consistency for a pair of views in each thread. Using a reasonably dense sampling, the kernel takes about 160ms for $n = 133$ projections at a achieved occupancy of 60% limited by 39 registers. On the CPU it would take > 1 second. This can be improved by handing a single value of κ in each thread and computing the consistency of a pair of views in each block. With the same settings, the improved kernel achieves an occupancy of 91% using 30 registers and takes 44ms to compute. We require only 26 registers when loading the matrices \mathbf{K}_0 and \mathbf{K}_1 into shared memory but are not faster. Algorithm 2 shows the sampling of the Radon derivative $\frac{\partial}{\partial t}\rho_{I_0}$ at I_0^κ in the inner-most loop. Algorithm 1 only shows the first half of the function body, because the same steps would be repeated with I_1^κ to obtain `sample1`. Note that this paper does not describe how to modulate the angle $d\kappa$ between individual epipolar planes so as to achieve an even sampling.

²<https://www5.cs.fau.de/research/software/epipolar-consistency>

V. CONCLUSION

This paper addresses the epipolar Consistency Conditions (ECC) of any two X-ray projections, which can be used for motion and calibration correction in FD-CT. We review an algorithm to measure the epipolar consistency and then simplify the geometric part of the algorithm analytically. We present a compact form, consisting of two 3×2 matrices, which can be computed from two source position in 12 lines of C-code. Accordingly, the computationally expensive part is reduced to multiplication by said matrices, conversion of the epipolar lines to angle and distance and two texture reads in the inner-most loop. Timing results of our GPU implementation provide a baseline for further optimizations. Future work might parametrize the Radon transform so as to avoid two `atan2` operations. As supplementary material, we provide an open-source example of the ECC algorithm. We hope that this work allows other groups interested in epipolar consistency to quickly adapt an efficient solution.

Acknowledgments: We are supported by the German Research Foundation; DFG MA 4898/3-1 “Consistency Conditions for Artifact Reduction in Cone-beam CT”.

REFERENCES

- [1] C. Debbeler, N. Maass, M. Elter, F. Dennerlein, and T. M. Buzug, “A new ct rawdata redundancy measure applied to automated misalignment correction,” in *Proceedings of the Fully 3D*, 2013, p. 264.
- [2] A. Aichert, N. Maass, Y. Deuerling-Zheng, M. Berger, M. Manhart, J. Hornegger, A. K. Maier, and A. Doerfler, “Redundancies in X-ray images due to the epipolar geometry for transmission imaging,” in *Proceedings of the third CT-meeting*, F. Noo, Ed., 2014, pp. 333–337.
- [3] M. S. Levine, E. Y. Sidky, and X. Pan, “Consistency conditions for cone-beam ct data acquired with a straight-line source trajectory,” *Tsinghua Sci Technol.*, vol. 15, no. 1, Feb 2010.
- [4] N. Maass, F. Dennerlein, A. Aichert, and A. Maier, “Geometrical Jitter Correction in Computed Tomography,” in *Proceedings of the third CT-meeting*, F. Noo, Ed., 2014, pp. 338–342.
- [5] R. Frysck and G. Rose, “Rigid motion compensation in interventional c-arm ct using consistency measure on projection data,” in *Proceedings of the MICCAI 2015*, ser. Lecture Notes in Computer Science, N. Navab, J. Hornegger, W. M. Wells, and A. F. Frangi, Eds., vol. 9349. Springer International Publishing, 2015, pp. 298–306.
- [6] A. Aichert, J. Wang, R. Schaffert, A. Dörfler, J. Hornegger, and A. Maier, “Epipolar consistency in fluoroscopy for image-based tracking,” in *Proceedings of the British Machine Vision Conference (BMVC)*, M. W. J. Xianghua Xie and G. K. L. Tam, Eds. BMVA Press, September 2015, pp. 82.1–82.10.
- [7] T. Grulich, W. Holub, U. Ha ler, A. Aichert, and A. Maier, “Geometric Adjustment of X-ray Tomosynthesis,” in *Proceedings of The 13th Fully 3D*, M. King, Ed., 2015, pp. 468–470.
- [8] A. Aichert, M. Berger, J. Wang, N. Maass, A. Doerfler, J. Hornegger, and A. Maier, “Epipolar consistency in transmission imaging,” *Medical Imaging, IEEE Transactions on*, vol. 34, no. 11, pp. 2205–2219, Nov 2015.
- [9] J. F. Blinn, “A homogeneous formulation for lines in 3 space,” *ACM SIGGRAPH Computer Graphics*, vol. 11, no. 2, pp. 237–241, Aug 1977.
- [10] S. S. Brandt, K. Hommelhoff Jensen, and F. Lauze, “Bayesian epipolar geometry estimation from tomographic projections,” in *Computer Vision - ACCV 2012*, K. M. Lee, Y. Matsushita, J. M. Rehg, and Z. Hu, Eds. Springer Berlin Heidelberg, 2012, pp. 231–242.